# Improvement of Automatic Hemorrhages Detection Methods using Brightness Correction on Fundus Images

Yuji Hatanaka[*a], Toshiaki Nakagawa[*b], Yoshinori Hayashi[*c], Masakatsu Kakogawa[*c], Akira Sawada[*d], Kazuhide Kawase[*d], Takeshi Hara[*b], Hiroshi Fujita[*b]
[a] Dept. of Electronic Control Engineering, Gifu National College of Technology
2236-2 Kamimakuwa, Motosu-shi, Gifu 501-0495, Japan
[b] Dept. of Intelligent Image Information, Division of Regeneration and Advanced Med. Science
Graduate School of Medicine, Gifu University, 1-1 Yanagido, Gifu-shi, Gifu 501-1194, Japan
[c] Tak Co., Ltd., 4-32-12 Kono, Ogaki-shi, Gifu 503-0803, Japan
[d] Dept. of Ophthalmology, Gifu University, School of Medicine
1-1 Yanagido, Gifu-shi, Gifu 501-1194, Japan

## ABSTRACT

We have been developing several automated methods for detecting abnormalities in fundus images. The purpose of this study is to improve our automated hemorrhage detection method to help diagnose diabetic retinopathy. We propose a new method for preprocessing and false positive elimination in the present study. The brightness of the fundus image was changed by the nonlinear curve with brightness values of the hue saturation value (HSV) space. In order to emphasize brown regions, gamma correction was performed on each red, green, and blue-bit image. Subsequently, the histograms of each red, blue, and blue-bit image were extended. After that, the hemorrhage candidates were detected. The brown regions indicated hemorrhages and blood vessels and their candidates were detected using density analysis. We removed the large candidates such as blood vessels. Finally, false positives were removed by using a 45-feature analysis. To evaluate the new method for the detection of hemorrhages, we examined 125 fundus images, including 35 images with hemorrhages and 90 normal images. The sensitivity and specificity for the detection of abnormal cases was were 80% and 88%, respectively. These results indicate that the new method may effectively improve the performance of our computer-aided diagnosis system for hemorrhages.

Keywords: pre-processing, detection, retinal fundus image, diabetic retinopathy, hemorrhage

## 1. INTRODUCTION

The detection of hemorrhages is one of the important factors in the early diagnosis of diabetic retinopathy (DR). The existence of hemorrhages is generally used to diagnose DR or hypertensive retinopathy by using the classification scheme of Scheie. In spite of detecting microaneurysms, it is difficult for ophthalmologists to find them in noncontrast fundus images. The contrast observed in a microaneurysm image is very low; therefore, ophthalmologists usually detect microaneurysms by using fluorescein angiograms. However, it is difficult to use fluorescein as a contrast medium for diagnosing all the medical examinees subjected to mass screening. Therefore, the patients who show the possibility of having DR were thoroughly examined at a hospital in Japan.

The number of patients with adult diseases such as diabetes and hypertension is on the rise in Japan. To prevent or detect these diseases in early stages, ophthalmologists rely on the examination of fundus images obtained from patients aged over 40 years during complete health examinations or mass screenings. DR is a complication associated with diabetes, and there is a high probability that diabetic patients will develop this condition within 10 years from the onset of diabetes. Furthermore, DR is the leading cause of blindness. In Japan, there are approximately 7.4 million patients with diabetes and approximately 16.2 million patients who may have diabetes [1]. Approximately three million are thought to suffer from DR. This disease can be prevented from developing into blindness if it is treated at an early stage.

*hatanaka@gifu-nct.ac.jp; phone 81 58 320 1384; fax 81 58 320 1263; gifu-nct.ac.jp

Medical Imaging 2008: Computer-Aided Diagnosis, edited by Maryellen L. Giger, Nico Karssemeijer
Proc. of SPIE Vol. 6915, 69153E, (2008) · 1605-7422/08/$18 · doi: 10.1117/12.771051

However, it has been recorded that approximately 3,000 people have lost their vision following the onset of DR. Fundus photographs obtained by the fundus camera are used to diagnose DR. Japanese ophthalmologists usually examine the presence of hemorrhages, microaneurysms, and exudates in order to diagnose DR.

Recently, many studies have been reported on the use of fundus images in the detection DR [2–9]. Niemeijer et al. proposed a method for the detection of microaneurysms in fluorescein angiograms [2–4]. Their method comprised two steps. Firstly, microaneurysms were detected by using a watershed transform. The false positives were then reduced by reliable vessel detection in the vicinity of each microaneurysms candidate. Serrano et al. proposed a method for detecting microaneurysms by the region growing technique in order to analyze fluorescein angiograms [5]. Usher et al. presented a method for detecting hemorrhages, microaneurysms, and exudates [6, 7]. The region growing method used by them segmented the abnormal and retinal regions. Nagayoshi et al. presented a method that included two additional processes to this method [8]. One of these was the normalization of the color pixel values and the other was the use of the color pixel values for blood vessels. Moreover, the previous method had the drawback of a long operation time of approximately 43 s per image [8].

We also reported a method for detecting hemorrhages and exudates in noncontrast fundus images [9]. Although the sensitivity for hemorrhages was 85%, the specificity was 21%. In our previous study, we had two problems—the absence of a technique to normalize fundus images and the removal of false positives. In this study, we aim to develop methods for fundus image normalization and false positive elimination method in the noncontrast images.

## 2. METHODS

### 2.1 Overall Scheme

The flowchart for our overall detection scheme is shown in Fig. 1. It consists of seven stages: (1) image digitization, (2) image normalization, (3) extraction of optic nerve head, (4) detection of hemorrhage candidates, (5) elimination of false positives in blood vessels, (6) elimination of funicular-shaped false positives, and (7) elimination of false positives by feature analysis. Further details are described below.

### 2.2 Image digitization

One hundred forty five fundus images were captured using a fundus camera and a flatbed-type scanner. Eighty seven fundus images were obtained at a resolution of an array of 1,600 × 1,600 pixels with 24-bit color, and 58 fundus images were obtained at a resolution of an array of 2,800 × 2,800 pixels with 24-bit color. An example of a color fundus image is shown in Fig. 2 (a).

Subsequently, the scale of the matrix was first reduced to the VGA size (width 640 pixels) by obtaining detailed subsamples from the original image data to improve processing efficiency.

### 2.3 Image normalization

Due to the flash, there is an atypical change in the color of the fundus images. We suggested a scheme of brightness correction using hue saturation value (HSV) space. First, the brightness values of the HSV space were calculated. The brightness correction value Bc(i, j) is given by the following equation:

$$Bc(i,j)=\sqrt{1-\{V(i,j)-1\}^2} \tag{1}$$

where $V(i, j)$ is the brightness value of the HSV space.

$$V(i,j)=MAX, \qquad MAX: R(i,j), G(i,j), B(i,j) \tag{2}$$

Next, the red value $R(i, j)$, green value $G(i, j)$, and blue value $B(i, j)$ changed by $Bc(i, j)$ are given by the following equation:

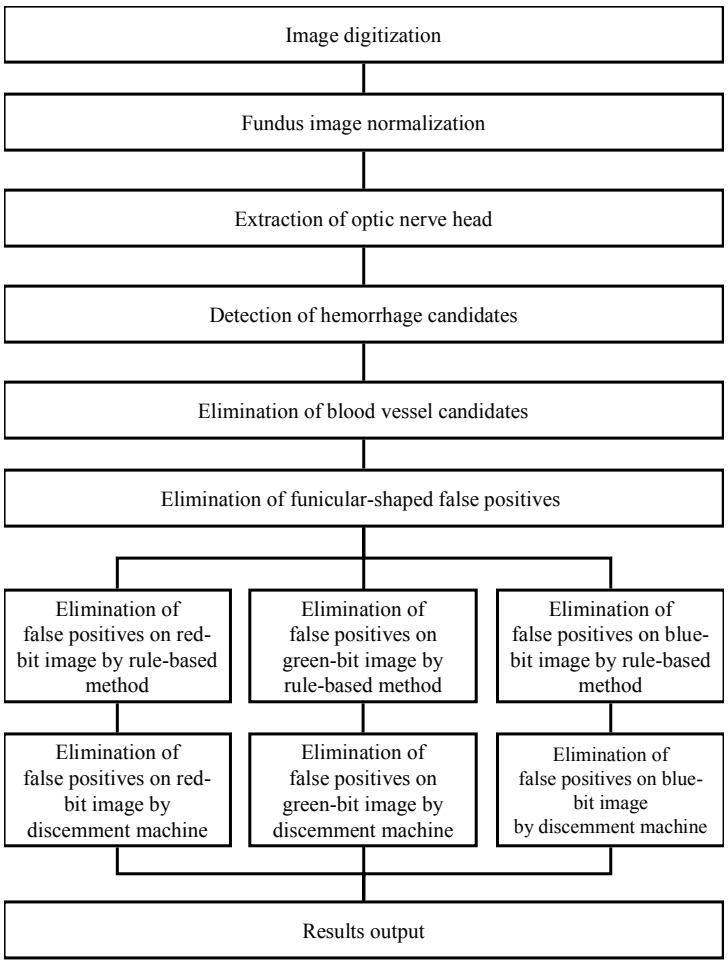


Fig. 1. Flowchart for detecting hemorrhages on fundus images.

$$H_i(i,j)=\left[\frac{H(i,j)}{60}\right]\bmod 6$$

$$f(i,j)=\frac{H(i,j)}{60}-H_i(i,j)$$

$$p(i,j)=V(i,j)[1-S(i,j)]$$

$$q(i,j)=V(i,j)[1-f(i,j)S(i,j)]$$

$$t(i,j)=V(i,j)\{1-[1-f(i,j)]S(i,j)\}$$

$$\begin{aligned}
&if \quad H_i(i,j)=0 \quad \rightarrow \quad R(i,j)=V(i,j), \quad G(i,j)=t(i,j), \quad B(i,j)=p(i,j)\\
&if \quad H_i(i,j)=1 \quad \rightarrow \quad R(i,j)=q(i,j), \quad G(i,j)=V(i,j), \quad B(i,j)=p(i,j)\\
&if \quad H_i(i,j)=2 \quad \rightarrow \quad R(i,j)=p(i,j), \quad G(i,j)=V(i,j), \quad B(i,j)=t(i,j)\\
&if \quad H_i(i,j)=3 \quad \rightarrow \quad R(i,j)=p(i,j), \quad G(i,j)=q(i,j), \quad B(i,j)=V(i,j)\\
&if \quad H_i(i,j)=4 \quad \rightarrow \quad R(i,j)=t(i,j), \quad G(i,j)=p(i,j), \quad B(i,j)=V(i,j)\\
&if \quad H_i(i,j)=5 \quad \rightarrow \quad R(i,j)=V(i,j), \quad G(i,j)=p(i,j), \quad B(i,j)=q(i,j)
\end{aligned} \tag{3}$$

where $H(i,j)$ is the hue value and $S(i,j)$ is the saturation value.

$$
\begin{aligned}
H &= \begin{cases} 60 \times \dfrac{G(i,j) - B(i,j)}{MAX - MIN} + 0, & if \quad MAX = R(i,j) \\ 60 \times \dfrac{B(i,j) - R(i,j)}{MAX - MIN} + 120, & if \quad MAX = G(i,j) \\ 60 \times \dfrac{R(i,j) - G(i,j)}{MAX - MIN} + 240, & if \quad MAX = B(i,j) \\ S = \dfrac{MAX - MIN}{MAX} \end{cases} \\
S &= \frac{MAX - MIN}{MAX} \\
MIN &: R(i,j), G(i,j), B(i,j)
\end{aligned} \tag{4}
$$

However, equation (2) cannot be used when $S(i,j)$ is zero. The brightness was equally corrected from the center to the skirt region of the fundus image (as shown in Fig.2 (b)). The color fundus images corrected by $Bc(i,j)$ were then processed by gamma correction. The gamma value was experimentally set to 1.5 (as shown in Fig.2 (c)). Finally, the histograms of each red, blue, and blue-bit were extended (as shown in Fig.2 (d)). The fundus images were standardized and made unclear by using these processes.

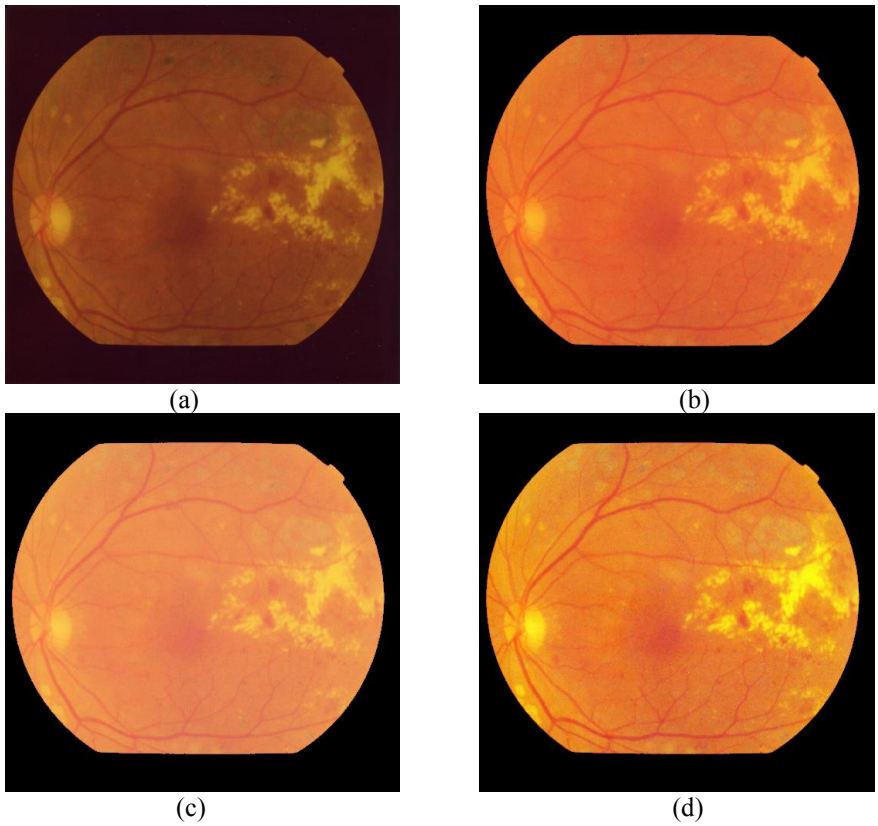


Fig. 2. Color contrast enhancement. (a) Original color fundus image. (b) Brightness of fundus image was changed by the nonlinear curve with brightness values of HSV space. (c) Image after processing by gamma correction. (d) Image was adjusted in the dynamic range.

### 2.4 Extraction of optic nerve head

The color images were converted into the grayscale images by selecting only the green component. Thus achieving a clearer contrast was obtained as compared to the original images, which included all the color components. After the optic nerve head was highlighted with brightness greater than that used for highlighting other tissues, it was investigated by the p-tile method [10]. The shape of the detected region was approximated to a circle.

### 2.5 Detection of hemorrhage candidates

The pixel values of hemorrhages in an image are lower than those of other regions. Therefore, the haemorrhages were detected by performing finite difference calculations along with smoothing. This method was carried out in two steps: the rough and detailed detection processes. Firstly, the fundus images were smoothed by using a mask of 3 × 3 pixels. Next, the difference in the pixel values between two smoothed images was calculated. Subsequently, the hemorrhage and blood vessel candidates were segmented by the thresholding technique. Fig. 3 (b) shows an image of the roughly detected vessels. As shown in this image, the end of thin vessels was not detected. Therefore, the end of the vessels was detected by using a similar method that uses two types of images smoothed with a mask of 9 × 9 pixels. Fig. 3 (c) shows an image of the detailed parts of the vessels. By combining both types of techniques for the detection of hemorrhages and vessels, we could detect all the blood vessels from the optic nerve head up to the end of the vessels. Fig. 3 (d) shows an image of the end of the vessels. Finally, the vessel candidates connected to the optic nerve head were eliminated (as shown in Fig. 3 (e)) and the vessel candidates with large or very small areas were eliminated. Fig. 3 (f) shows an example of a resulting image.

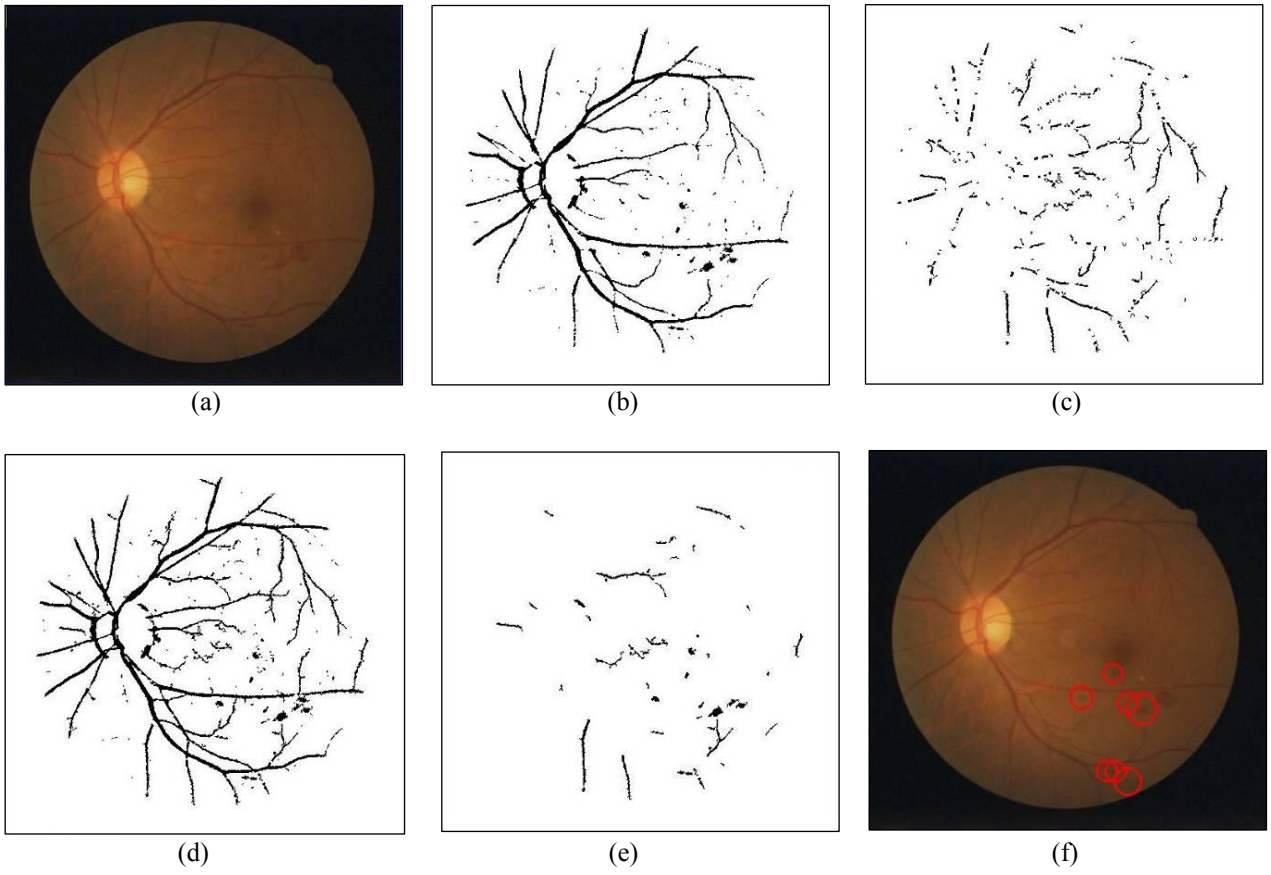


Fig. 3. Illustration of the hemorrhage detection processes. (a) Input image. (b) Roughly detected hemorrhages and blood vessels. (c) Details of detected hemorrhages and blood vessels. (d) Combination of (b) and (c). (e) Candidates connecting blood vessels and candidate with large areas were eliminated. (f) Final image of hemorrhage detection.

**2.6 Elimination of incorrectly detected vessels**

The images of the retinal vessel include those reflected from the arterial wall. Further, the fundus images were obscured due to cataract. Therefore, it was difficult to detect all the vessels up to the end by using the method proposed in section **2.5**. We can resolve such difficulties by changing the threshold value proposed in section **2.5**. However, the hemorrhage candidates were connected to the vessel candidates. Therefore, our method could not separate the connected candidates into hemorrhage and vessel candidates. The measures taken to resolve this problem can be described as follows.

Firstly, the threshold value was selected in such a manner that the vessels could be continuously detected. The centerlines of the vessels were extracted by using a thinning technique. Subsequently, the centerlines with large areas were extracted in such a manner that the hemorrhage candidates could not be extracted. Finally, the vessels extracted with the centerlines were eliminated in order to avoid the vessels from being incorrectly detected.

**2.7 Elimination of funicular shapes**

All the false positives on the vessels were not eliminated by the method proposed in section **2.6.** Hence, the remaining false positives were eliminated by evaluating the length-to-width ratio. The value of this ratio was small when the candidate was incorrectly detected as a vessel. The details of the evaluation can be described as follows. Firstly, the minimum rectangular region that surrounds the candidates was determined. The angle of the hemorrhage candidate was then determined by calculating the moment so that the *X* and *Y* axes could be determined by using the obtained angle. Subsequently, binarized images were projected on the *X* and *Y* axes. By examining each of the projected images, the positions *Xa*, *Xb*, *Ya*, and *Yb* were determined. In this way, we could specify the black and white regions. Finally, we could determine the length-to-width ratio, denoted by *LW*, using the following equation:

$$LW = \frac{\min(|X_a - X_b|, |Y_a - Y_b|)}{\max(|X_a - X_b|, |Y_a - Y_b|)} \tag{5}$$

where min(|Xa–Xb|,| Ya–Yb |) is the mean value of the width, and max(|Xa–Xb|,| Ya–Yb |) is the mean value of the length.

**2.8 Elimination of false positives by feature analysis**

The minimum rectangular region that surrounds the hemorrhage candidates extends beyond five pixels in each direction along the *X* and *Y* axes. Next, the average pixel values inside and outside the candidate region were calculated. Further, the contrast was determined by evaluating the ratio between the two average values.

Furthermore, we proposed a cascade classification process.

At first, the false positives were eliminated by a rule-based method using 45 features. Typical false positives were eliminated in this step. We extracted the following 15 features from the rectangular regions: 12 features calculated from the co-occurrence matrix [11], two features based on gray-level difference statistics [12], and one feature determined by the extrema method [13]. The 12 features from the co-occurrence matrix were (1) angular second moment, (2) contrast, (3) correlation, (4) sum of squares, (5) inverse difference moment, (6) sum average, (7) sum variance, (8) sum entropy, (9) entropy, (10) difference variance, (11) difference entropy, and (12) information measurements for correlation. The two features based on gray-level difference statistics were (a) angular second moment and (b) mean. The minimum rectangular region that surrounds the candidates was determined. These features were calculated in the rectangular regions in the three grey-level images, which comprised red, green, and blue-bit images.

Finally, the false positives were eliminated by employing the discemment machines and using Mahalanobis distances [14]. It was used suggested three Mahalanobis' distances by using above 15 features from the rectangular regions in the three grey level images.

## 3. RESULTS AND DISCUSSIONS

The contrast of hemorrhages in the images was enhanced. The contrast of the processed image (as shown in Fig. 4 (c)) was higher than that of the original image (as shown in Fig. 4 (b)). Moreover, the color of the processed image was

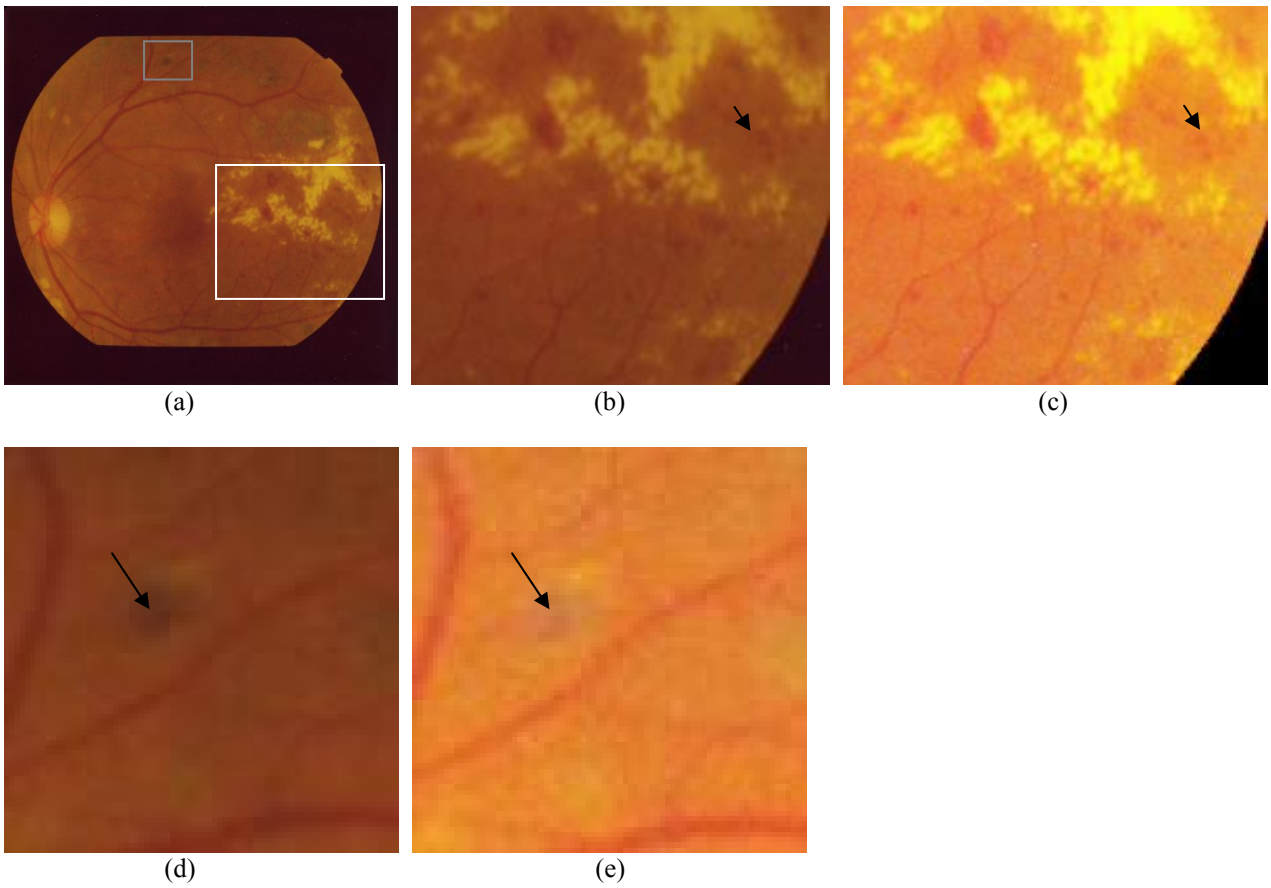


Fig. 4. Process of hemorrhage enhancement. (a) Original image. (b) Enlarged image of the region indicated by the white rectangle in (a). Black arrow shows the hemorrhage. (c) Enhanced image of (b). (d) Enlarged image of the region indicated by the gray rectangle in (a). Black arrow shows the laser mark. (e) Enhanced image of (d).

standardized by the histogram extended method. However, if the fundus image has some laser marks, the marks are changed blighter and more obscure than the original color pixel (as shown in Fig.4 (d) and (e)).

We set some parameters experimentally by using 20 fundus images with hemorrhage. The sensitivity was 95% (19/20). To eliminate the incorrectly detected hemorrhages, we used 45 calculated features. One hundred and twelve hemorrhages were detected with 630 false positives in 20 fundus images. Table 1 shows the number of false positives eliminated by using the rule-based method. In Table 1, the most effective grey-scale image is the green-bit image. Moreover, the most valid feature was the information measure of correlation from the co-occurrence matrix for the green-bit image, which could eliminate 74 false positives (12%) by the rule-based method. However, four features in the green-bit image could not eliminate one for false positive. When we used 45 features for the elimination of false positives, 166 false positives (26%) were eliminated without the loss of a true positive.

Then, we constructed a discemment machine by using Mahalanobis distances; we used 45 features for each grey-scale image (as shown in Table 2). When we constructed a discemment machine by using 112 true positives and 630 false positives, 117 false positives (19%) were eliminated. Table 2 shows that the most effective image is the blue-bit one, though Table 1 showed the most effective image was green-bit one. We think that the worst features that were ineffective had a negative influence on the discemment machine with regard to the green-bit image.

Subsequently, 219 false positives (35%) were eliminated using a rule-based method and three discemment machines by Mahalanobis' distances.

Finally, to evaluate our method of detecting hemorrhages, we examined 125 fundus images; hemorrhages were detected in 35 images, and no abnormal cases were detected in the remaining 90 images. By using our scheme, we

succeeded in obtaining satisfactory results with a sensitivity of 80% (28/35) when the specificity was 88% (79/90). Our scheme could not detect any hemorrhages. The main reason was that hemorrhages that touched the blood vessel were undetectable. Our algorithm was not able to separate the blood vessel regions and hemorrhage regions, and therefore such hemorrhages were removed together with the blood vessels (discussed in section **2.6**).

Table 1. The false positives were eliminated by 45 rule-based methods.

| Features | Red | Green | Blue |
|---|---|---|---|
| Extrema | 19 | 9 | 1 |
| CM: Angular second moment | 3 | 26 | 6 |
| Contrast | 25 | 5 | 12 |
| Correlation | 3 | 8 | 16 |
| Sum of squares | 24 | 37 | 7 |
| Inverse difference moment | 4 | 2 | 8 |
| Sum average | 3 | 3 | 10 |
| Sum variance | 23 | 0 | 11 |
| Sum entropy | 24 | 0 | 14 |
| Entropy | 23 | 7 | 9 |
| Difference variance | 26 | 0 | 14 |
| Difference entropy | 23 | 0 | 12 |
| Information measurements | 39 | 74 | 17 |
| GD: Angular second moment | 3 | 2 | 11 |
| Mean | 28 | 5 | 12 |
| Subtotal | 58 | 105 | 44 |
| Total | | | 166 |

CM: co-occurrence matrix, GD: gray-level difference statistics

Table 2. The false positives were eliminated by three discemment machines using Mahalanobis distances.

| | Red | Green | Blue |
|---|---|---|---|
| Discemment machine | 52 | 17 | 64 |
| Three discemment machines combined | | | 117 |
| Forty five rule-based methods and Three discemment machines combined | | | 219 |

## 4. CONCLUSION

In this study, a new scheme for automatically detecting hemorrhages is presented by using digitized noncontrast fundus images as an example. This scheme can be applied to the computer-aided diagnosis (CAD) system for diagnosing eye diseases. The results of the preliminary testing showed a desirable consistency with those obtained from the proposed scheme. It was demonstrated that the algorithm detected abnormalities with high accuracy and reliability. The result of the initial work on fundus images clarified that the efficiency and accuracy of the diagnosis of DR was considerably improved. The results of this study will be sent to ophthalmologists for further evaluation. The efficiency and accuracy of the diagnosis of DR was improved due to the detection of hemorrhages with a high accuracy. The application of the proposed scheme to fundus images enhances the CAD system performance for detecting hemorrhages in fundus images.

We have been attempting to develop a synthetic fundus CAD system [15–22]. We reported methods of detecting abnormal blood vessels to help in the diagnosis of hypertensive retinopathy [15–18]. Moreover, we proposed a method of detecting retinal nerve fiber layer defects (NFLD) [19] and a method of calculating the cup to disc ratio (C/D ratio) [20] to help in the diagnosis of glaucoma. In addition, we proposed a technique to obtain the depth value from the stereo image pair of a retinal fundus for the 3-D reconstruction of the optic nerve head [21, 22]. In the future, the integrated analysis scheme will be further improved and more clinical cases will be reported for evaluating its accuracy. The techniques employed in our system will help in improving diagnostic accuracy as well as in reducing the workload of ophthalmologists in the future.

## ACKNOWLEDGMENTS

The authors thank T. Yamamoto, A. Fujita, Y. Mizukusa, T. Suzuki, T. Kunieda, K. Sugio, N. Kajima, M. Okamoto, H. Mutoh, and H. Nonogaki for their significant contributions to this study.

This work was supported in part by "Knowledge-based Clusters" from the MEXT, Japan.

## REFERENCES

1. Health and Welfare Statistics Association, *Journal of Health Welfare Stat*., **51**, 144–148, 2004.
2. M. Niemeijer, B. V. Ginneken, J. Staal, M. S. Suttorp-Schulten, and M. D. Abramoff, "Automatic detection of red lesions in digital color fundus photographs," *IEEE Transactions on Medical Imaging*, **24 (5)**, 584–592, 2005.
3. A. J. Framea, P. E. Undrill, M. J. Cree, J. A. Olson, K. C. McHardy, P. F. Sharp, and J. V. Forrester, "A comparison of computer based classification methods applied to the detection of microaneurysms in ophthalmic fluorescein angiograms," *Computers in Biology and Medicine*, **28 (3)**, 225–238, 1998.
4. A. D. Fleming, S. Philip, K. A. Goatman, J. A. Olson, and P. F. Sharp, "Automated microaneurysm detection using local contrast normalization and local vessel detection," *IEEE Transactions on Medical Imaging*, **25 (9)**, 1223–32, 2006.
5. C. Serrano, B. Acha, and S. Revuelto, "2D adaptive filtering and region growing algorithm for the detection of microaneurysms," *Proceedings of SPIE Medical Imaging 2007: Image Processing*, **5370**, 1924–1931, 2004.
6. C. Sinthanayothin, J. F. Boyce, T. H. Williamson, H. L. Cook, E. Menshan, S. Lal, and D. Usher, "Automated detection of diabetic retinopathy on digital fundus images," *Diabetic UK Diabetic Medicine*, **19 (1)**, 105–112, 2002.
7. D. Usher, M. Dumskyj, M. Himaga, T. H. Williamson, S. Nussey, and J. F. Boyce, "Automated detection of diabetic retinopathy in digital retinal images: a tool for diabetic retinopathy screening," *Diabetic UK Diabetic Medicine*, **21 (1)**, 84–90, 2004.
8. H. Nagayoshi, Y. Hiramatsu, T. Kagehiro, Y. Mizuno, M. Himaga, H. Sakou, S. Sato, H. Fukushima, and S. Kato, "Detection of lesions from fundus images for diagnosis of diabetic retinopathy," *IEICE Technical Report*, **105 (64)**, 61–66, 2005.
9. W. Doyle, "Operation useful for similarity-invariant pattern recognition," *Journal of Association for Computing Machinery*, **9 (2)**, 259–267, 1962.
10. Y. Hatanaka, T. Nakagawa, Y. Hayash, A. Fujita, Y. Mizukusa, M. Kakogawa, K. Kawase, T. Hara, and H. Fujita, "CAD scheme for detection of hemorrhages and exudates in ocular fundus images," *Proceedings of SPIE Medical Imaging 2007: Computer-aided Diagnosis*, **6514**, 65142M-1-65142M-8, 2007.
11. R. M. Haralick, "Statistical and structural approaches to texture," *Proceeding of the IEEE*, **67 (5)**, 786-804, 1979.
12. J. S. Weszka, C. R. Dyer, and A. Rosenfeld, "A comparative study of texture measures for terrain classification," *IEEE Transactions on Systems, Man, and Cybernetics*, **SMC-6 (4)**, 269–285, 1976.
13. O. R. Mitchell, C. R. Myers, and W. Boyne, "A max-min measure for image texture analysis," *IEEE Transactions on Computers*, **C-2 (4)**, 408–414, 1977.
14. M. Iwamura, S. Omachi, and H. Aso, "Character recognition with Mahalanobis distance based on between-cluster information," *IEICE Technical Report*, **98 (490)**, 49–54, 1998.
15. Y. Hatanaka, T. Hara, H. Fujita, M. Aoyama, H. Uchida, and T. Yamamoto, "Automatic distribution and shape analysis of blood vessels on retinal images," *Proceedings of SPIE Medical Imaging 2007: Image Processing,* **5370**, 1621–1628, 2004.

16. Y. Hatanaka, X. Zhou, T. Hara, H. Fujita, Y. Hayashi, A. Aoyama, and T. Yamamoto, "Automated detection algorithm for abnormal vessels on retinal fundus images," *Proceedings of the 10th International Conference on Virtual Systems and MultiMedia* (*VSMM2004*), 303–306, 2004.
17. Y. Hatanaka, T. Nakagawa, Y. Hayashi, A. Aoyama, X. Zhou, T. Hara, H. Fujita, Y. Mizukusa, A. Fujita, and M. Kakogawa, "Automated detection algorithm for arteriolar narrowing on fundus images," *Proceedings of the 2005 IEEE Engineering in Medicine and Biology 27th Annual Conference*, paper#291, 2005.
18. R. Takahashi, Y. Hatanaka, T. Nakagawa, Y. Hayashi, A. Aoyama, Y. Mizukusa, A. Fujita, M. Kakogawa, T. Hara, and H. Fujita, "Automated analysis of blood vessel intersections in retinal images for diagnosis of hypertension," *Medical Imaging Technology*, **24 (4)**, 270–276, 2006.
19. Y. Hayashi, T. Nakagawa, Y. Hatanaka, A. Aoyama, Y. Mizukusa, A. Fujita, M. Kakogawa, T. Hara, H. Fujita, and T. Yamamoto, "Detection of retinal nerve fiber layer defects in retinal fundus images using Gabor filtering," *Proceedings of SPIE Medical Imaging 2007: Computer-aided Diagnosis*, **6514**, 65142Z-1-65142Z-8, 2007.
20. Y. Hatanaka, Y. Hayashi, T. Nakagawa, A. Aoyama, X. Zhou, T. Hara, H. Fujita, Y. Mizukusa, A. Fujita, and M. Kakogoawa, "Development of Computer-aided Diagnosis System for Fundus Images," *8th International Conference on Medical Image Computing and Computer-assisted Intervention: Short Paper, Oct., 2005,* http://www.miccai2005.org, 2005.
21. T. Nakagawa, Y. Hayashi, Y. Hatanaka, A. Aoyama, T. Hara, M. Kakogawa, H. Fujita, and T. Yamamoto, "Comparison of the depth of an optic nerve head obtained using stereo retinal images and HRT," *Proceedings of SPIE Medical Imaging 2007: Physiology, Function, and Structure from Medical Images*, **6511**, 65112M-1-65112M-9, 2007.
22. T. Nakagawa, Y. Hayashi, Y. Hatanaka, A. Aoyama, T. Hara, A. Fujita, M. Kakogawa, H. Fujita, and T. Yamamoto, "Three-dimensional reconstruction of optic nerve head from stereo fundus images and its quantitative estimation," *Proceedings of 29th IEEE Engineering in Medicine and Biology Conference Management System Annual International Conference*, 6747–6750, 2007.